JACS
JOURNAL OF THE AMERICAN CHEMICAL SOCIETY
Article
pubs.acs.org/JACS

A Ru(I) Metalloradical That Catalyzes Nitrene Coupling to Azoarenes from Arylazides

Ayumi Takaoka, Marc-Etienne Moret, and Jonas C. Peters*

California Institute of Technology, Division of Chemistry and Chemical Engineering, Pasadena, California 91125, United States

Supporting Information

ABSTRACT: Unusual N−N coupling of aryl azides to yield azoarenes is demonstrated by the Ru(I) metalloradical, [SiP$^{iPr}_3$]Ru(N$_2$) (**4**) ([SiP$^{iPr}_3$] = (2-*i*Pr$_2$PC$_6$H$_4$)$_3$Si$^-$). The yield of the azoarene is dependent on the substituent on the aryl azide, and the reaction is catalytic for *p*-methoxy and *p*-ethoxy phenyl azides, while no azoarene is observed for *p*-trifluoromethylphenyl azide. Studies aimed at probing the viability of a bimolecular coupling mechanism of metal imide species, as shown in the related [SiP$^{iPr}_3$]Fe system, have led to the isolation of several structurally unusual complexes including the ruthenium(IV) imide, **7-OMe**, as well as the Ru(II) azide adduct **8-OMe**. One electron reduction of **7-OMe** complex led to the isolation of the formally Ru(III) imide complex, [SiP$^{iPr}_3$]Ru(NAr) (Ar = *p*-MeOC$_6$H$_4$, **5-OMe**). EPR spectroscopy on **5-OMe** suggests that the complex is electronically similar to the previously reported imide complex, [SiP$^{iPr}_3$]Ru(NAr) (Ar = *p*-CF$_3$C$_6$H$_4$, **5-CF$_3$**), and features radical character on the NAr moiety, but to a greater degree. The stability of **5-OMe** establishes that bimolecular coupling of **5-OMe** is kinetically inconsistent with the reaction. Further studies rule out mechanisms in which **5-OMe** reacts directly with free aryl azide or a transient Ru(I) azide adduct. Together, these studies show that **5-OMe** is likely uninvolved in the catalytic cycle and demonstrates the influence of the metal center on the mechanism of reaction. Instead, we favor a mechanism in which free aryl nitrene is released during the catalytic cycle and combines with itself or with free aryl azide to yield the azoarene.

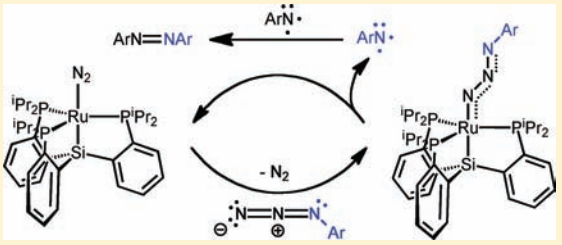

1. INTRODUCTION

Organic azides are valuable sources of nitrenes (NR). They are easily synthesized for a wide array of R substitutents and release N$_2$ as the only byproduct. These aspects make organic azides preferable for nitrene transfer/insertion in organic synthesis over hypervalent iodine compounds (PhI=NTs, etc.) and N-halogenated sulfonamides (chloramine-T, bromamine-T),[1−3] which have received more attention but are less flexible with respect to substituent variability and/or release of undesirable byproducts. As a result, recent efforts have increasingly focused on developing metal catalyzed nitrene transfer reactions with organic azides.[4] Because the commonly invoked intermediate in these reactions is the metal nitrene/imide species, its reactivity and mechanism of formation from the precursor metal azide adduct have been an important topic of study.

Well-defined metal azide complexes are relatively uncommon species and their decay has been mechanistically examined in limited cases. Bergman and Cummins were the first to report such studies. Bergman's Cp$_2$Ta(CH$_3$)(N$_3$Ar) complexes were found to decay cleanly in a unimolecular fashion to afford the corresponding imide complexes, Cp$_2$Ta(CH$_3$)(NAr),[5] akin to N$_2$ extrusion in phosphazides (ArN$_3$PR$_3$) that proceeds through a four-membered transition state to yield iminophosphoranes.[6] Cummins' V(N$_3$Mes)(I)(NRAr$_F$)$_2$ (Ar$_F$ = 2,5-C$_6$H$_3$FMe) system, in contrast, followed bimolecular decay to the corresponding imide complex, V(NMes)(I)(NRAr$_F$)$_2$.[7] In both studies, the γ-N atom of the azide ligand is bound to the metal center in the precursor complex and, indeed, this is the most commonly observed binding mode for structurally characterized azide complexes.[5,7,8,10] A more recent mechanistic study by Hillhouse described an unusual η^2 bound azide complex, (dtbpe)Ni(N$_3$R) (dtbpe = bis(ditert-butylphosphino)ethane, R = adamantyl), that decayed unimolecularly to the imide complex, (dtbpe)Ni(NR). In this study, a large and negative entropy of activation was observed, consistent with a highly ordered transition state.[9]

Our group has recently studied the interaction between aryl azides and the Fe(I) complex, [SiP$^{iPr}_3$]Fe(N$_2$) (**1**).[10,11] This reaction was found to initially form an Fe(I) azide adduct, [SiP$^{iPr}_3$]Fe(N$_3$Ar) (**2**), which subsequently exhibited clean unimolecular decay as in the Bergman and Hillhouse systems. Interestingly, the major product of this decay was shown to be azoarene and **1**, and use of excess aryl azide demonstrated catalytic azoarene formation from **1**. While several stoichiometric reactions had been known,[12] this example was noteworthy in that it represented a rare example of catalytic N−N coupling to yield azoarene from organic azides, and the first in which azoarene was the major product.[13] Mechanistic studies suggested the formation of a transient Fe(III) imide complex, [SiP$^{iPr}_3$]Fe(NAr) (**3-R**), following decay of **2**, which subsequently underwent 4e$^-$ reductive N−N coupling to produce azoarene (Scheme 1).[14]

Received: December 12, 2011
Published: March 1, 2012

   dx.doi.org/10.1021/ja211603f | J. Am. Chem. Soc. 2012, 134, 6695−6706

Scheme 1. Catalytic Azobenzene Formation with 1

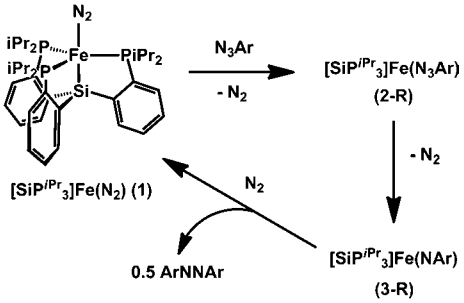

Complex **3-R** is a reactive species that was only observable by EPR spectroscopy in a frozen glass (for R = tol). While the EPR features of **3-R** were indicative of an S = 1/2 ground state, DFT calculations predicted a small doublet-quartet gap of 2.8 kcal/mol, perhaps suggesting that two-state reactivity[15] may be responsible for its rich reactivity; this included hydrogen atom abstraction from 9,10-dihydroanthracene and carbodiimide formation with *t*-butylisocyanide.[10] In this regard, the recent isolation of the Ru(I) metalloradical, $[SiP^{iPr}_3]Ru(N_2)$ (**4**), and its interaction with *p*-$CF_3C_6H_4N_3$ to yield the formally Ru(III) imide complex, $[SiP^{iPr}_3]Ru(NC_6H_4CF_3)$ (**5-CF$_3$**), is noteworthy (Scheme 2).[16] This work highlighted the first reaction

Scheme 2. Synthesis of 5-CF$_3$ from 4

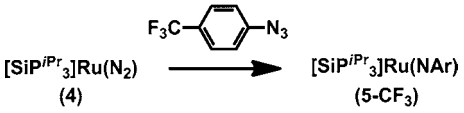

chemistry of an unusual mononuclear ruthenium(I) complex. Although **5-CF$_3$** did not yield azoarene upon decay, it was stable enough for thorough characterization. We thus envisioned that use of other substituted aryl azides might yield similar metal imide species (**5-R**) that would retain some stability for characterization, yet also exhibit N−N coupling reactivity as observed in the Fe system. Further, because the doublet-quartet gap in the heavier congeners of **1** is expected to be much greater than **1**, any azoarene formation in the Ru system could also be used as indirect support for doublet state involvement in **3-R**,[17] provided that the same mechanism is operative in both systems.

We herein report the results of our studies on **4** with substituted aryl azides. The key compounds involved are shown in Figure 1 for reference. The tendency of the aryl azide to degrade in the presence of **4** to azoarene product, either stoichiometrically or catalytically, is dependent on the aryl-ring substitution pattern. Terminally bonded $[SiP^{iPr}_3]Ru(NAr)$ complexes **5-R** were observed in some stoichiometric reactions and independent synthesis of **5-OMe** allowed thorough characterization and detailed mechanistic studies. Contrary to our initial expectation, we establish that species **5-R** is not responsible for the observed reactivity and instead determine that a dramatic change in mechanism occurs in moving from Fe to Ru within the $[SiP^{iPr}_3]M(N_2)$ system.

2. RESULTS AND DISCUSSION

2.1. Reaction between 4 and *p*-MeOC$_6$H$_4$N$_3$ and Other Aryl Azides. Addition of 1 equiv of *p*-$MeOC_6H_4N_3$ to **4** in Et_2O yielded the substituted azoarene, ArN═NAr (Ar = *p*-

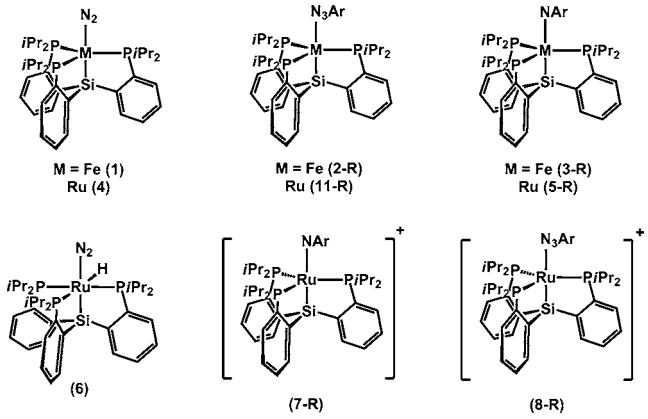

Figure 1. Key compounds involved in this work. Lines between core atoms only denote connectivity.

$MeOC_6H_4$), in 93(7) % yield as judged by ^{1}H NMR spectroscopy with ferrocene (Fc) as an internal standard (Scheme 3). The major metal containing product was **4**, with

Scheme 3. Azoarene Formation Catalyzed by 4

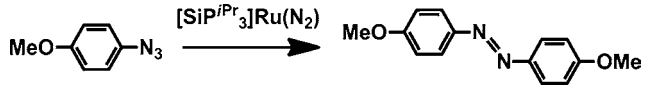

small amounts of previously reported[16] $[SiP^{iPr}_3]Ru(H)(N_2)$ (**6**) and a minor paramagnetic product, which will be shown below to be the imide species, **5-OMe**. In contrast to the Fe system, which required heating at 70 °C, the reaction between *p*-$MeOC_6H_4N_3$ and **4** was complete within seconds at room temperature. As **4** was the major metal containing product in the stoichiometric reaction, catalysis could be expected and addition of 10 equiv of *p*-$MeOC_6H_4N_3$ led to catalytic generation of roughly 50% yield of azoarene with catalyst decomposition. Low temperature ^{1}H NMR studies showed that azoarene began to form at about −65 °C, and no obvious buildup of intermediates was observed; the broadness of the paramagnetic resonances prevented our ability to draw any definitive conclusions about the metal containing species present in solution at these temperatures. Performing the reaction in the presence of excess elemental mercury (>500 equiv) had little effect, suggesting that colloidal metal is unlikely to be responsible for the catalysis.

Use of other para-substituted aryl azides showed that the electronic influence of the substituent, R, on the phenyl group greatly affected the yield of azoarene. Similar to R = OMe, use of azide with R = OEt led to near quantitative yield of azoarene (Table 1). Use of aryl azides where the aryl group is either a

Table 1. Yield (%) of ArNNAr from 4 and 1 equiv of Substituted ArN$_3$

R =	*p*-OEt	*p*-OMe	Mes	*p*-Me	*p*-CF$_3$
ArNNAr	91(9)	93(7)	42(3)	29(1)	0

mesityl or a *p*-tolyl substituent, in contrast, led to diminished yields of azoarene with greater amounts of **6**. Finally, as previously reported, R = CF_3 did not yield any azoarene but exclusively provided **5-CF$_3$**. Thus, electron donating groups increase the yield of azoarene formation. Because the aryl azide para-substituted by R = OMe gave the highest yield of

dx.doi.org/10.1021/ja211603f | J. Am. Chem. Soc. 2012, 134, 6695−6706

azoarene, this aryl azide provided the main focus of subsequent mechanistic studies.

2.2. A Strategy toward the Synthesis of 5-OMe. We have previously concluded that Fe(III) imide complexes bimolecularly couple to yield azoarenes in the $[SiP^{iPr}_3]Fe$ system.[10] We thus conducted experiments to probe whether such species were also responsible for azoarene formation in this Ru system. Mechanistic analysis in this study, however, was complicated by the presence of multiple paramagnetic species. Since no buildup of intermediates was observed during low-temperature NMR experiments, attempts to independently synthesize **5-OMe** were made to assess the viability of **5-OMe** as a chemically and kinetically competent species for the nitrene coupling process. In this context, it is noteworthy that **5-CF$_3$** features a reversible oxidation event at −1.0 V (vs Fc/Fc^+, see Supporting Information (SI)). Chemical oxidation of **5-CF$_3$** with AgOTf cleanly led to the Ru(IV) imide complex, $\{[SiP^{iPr}_3]Ru(NAr)\}OTf$ (**7-CF$_3$**). This compound is thermally robust and represents an unusual example of a structurally characterized (see SI) terminal imide of Ru(IV).[18] The increased thermal stability of **7-CF$_3$** relative to **5-CF$_3$** pointed to increased stability of **7-OMe** relative to **5-OMe**. We thus aimed at first synthesizing **7-OMe**, which would enable chemical reduction to **5-OMe**. Since the stoichiometric reactions in this Ru system were complete within seconds at room temperature, complex **5-OMe** would be expected to rapidly yield azoanisole upon reduction from **7-OMe** if the same mechanism as in the Fe system were at play (Scheme 4).

Scheme 4. Strategy for Probing the Decay of 5-OMe

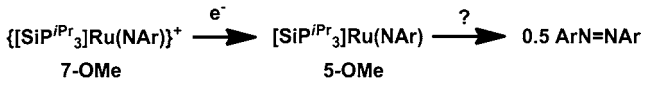

Addition of 1 equiv of *p*-$MeOC_6H_4N_3$ to previously reported[16] $\{[SiP^{iPr}_3]Ru(N_2)\}BAr^F_4$ (**9-BAr$^F_4$**) resulted in a rapid color change from orange to red, yielding the diamagnetic Ru(II) azide adduct, $\{[SiP^{iPr}_3]Ru(N_3Ar)\}BAr^F_4$ (**8-OMe**) (Scheme 5). Both the ^1H and $^{31}P\{^1H\}$ NMR spectra are consistent with a 3-fold symmetric structure on the NMR time scale. The diamagnetic spectra are suggestive of a distorted 5-coordinate structure that lies between a square pyramid (SP) and trigonal bipyramid (TBP) (vide infra), as seen in other structurally characterized d^6 ruthenium complexes of $[SiP^R_3]$ (R = *i*Pr, Ph).[16,19] The IR spectrum of **8-OMe** exhibits a strong N−N stretch at 2106 cm^{-1}. This value is close to the value of free *p*-$MeOC_6H_4N_3$ (2103 cm^{-1}), and is in accord with an unactivated azide ligand as expected for a cationic Ru(II) complex. Upon photolysis of **8-OMe** with a mercury lamp in the presence of excess azide, a color change from red to green took place and the $^{31}P\{^1H\}$ signal of **8-OMe** at 72 ppm decreased as a new peak at 106 ppm gained in intensity. Monitoring the complete decay of the signal at 72 ppm and following with workup yielded diamagnetic and green **7-OMe** in good yield. Consistent with N_2 loss, the IR spectra of **7-OMe** showed no significant stretch near 2100 cm^{-1} after photolysis.

Scheme 5. Synthesis of 5-OMe

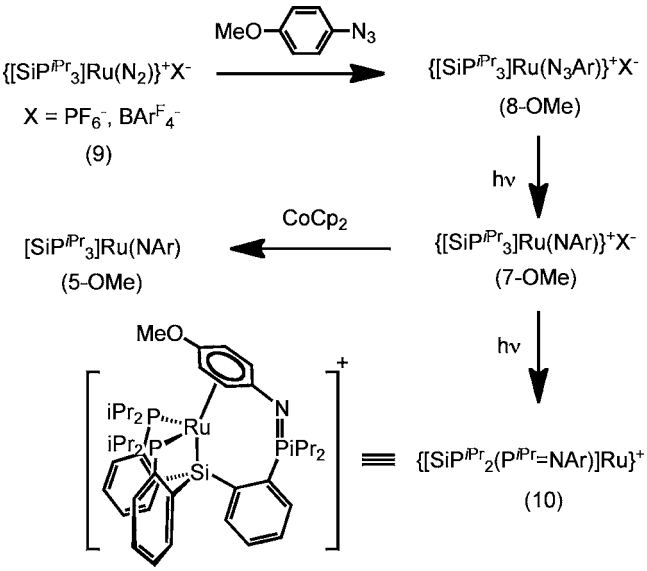

Interestingly, new signals at 86, 79, and 33 ppm in the $^{31}P\{^1H\}$ spectrum developed at the expense of the signal for **7-OMe** upon prolonged photolysis. The conversion was complete after two days and X-ray diffraction studies (vide infra) revealed nitrene insertion into the Ru−P bond of **7-OMe** and binding of the aryl ring in the nitrene moiety to the metal center in an η^6 mode (complex **10**, Scheme 5). The ^1H NMR spectrum of the nitrene insertion product **10** exhibits three resonances between 6.7 and 5.3 ppm that correspond to the resonances of the η^6 arene moiety. The $^{31}P\{^1H\}$ resonance at 33 ppm is attributed to the oxidized phosphine center. For ease of purification, subsequent studies utilized the PF_6^- anion for **7-OMe**, **8-OMe**, and **9**. These were synthesized in the same manner as the $BAr^F_4^-$ anion complexes (Scheme 5), except for **9-PF$_6$**, which was synthesized by oxidation of **4** with $AgPF_6$ (see Experimental Section).

2.3. Solid-State Structures of 8-OMe, 7-OMe, and 10. The solid-state structures of **8-OMe**, **7-OMe**, and **10** have been obtained and are shown in Figure 2. The geometry about the metal center in **8-OMe** is between that of a trigonal bipyramid and a square pyramid with a τ value[20] of 0.39. The N(1)−N(2) and N(2)−N(3) distances of 1.107(5) and 1.254(6) Å are short and similar to the values of crystallographically characterized free organic azides.[21] The N(1)−N(2) distance in **8-OMe** is significantly shorter than the bond distance in the Fe(I) azide adduct,[10] **2-Ad** (1.27(1) Å), suggesting little activation of the azide ligand. The near linear N(1)−N(2)−N(3) angle of 168.3(6) is also in contrast to **2-Ad** (147(4)°) but similar to the value of 173.1(3)° observed in a Cu(I) azide complex, $[HB(3,5\text{-}(CF_3)_2Pz)_3]Cu(N_3Ad)$ ($[HB(3,5\text{-}(CF_3)_2Pz)_3]^-$ = hydridotris(3,5-bis(trifluoromethyl)pyrazolyl)-borate).[8f] Interestingly, **8-OMe** appears to be the only crystallographically characterized ruthenium complex with a coordinated organic azide reported to date.

The solid-state structure of **7-OMe** features a metal center with a τ value of 0.90, approximating a trigonal bipyramidal geometry. The ruthenium is significantly displaced out of the plane of the phosphines, however, and the three P−Ru−P angles sum to 340.93(5)°. The Ru−Si bond length of 2.491(1) Å is accordingly much longer than typically observed distances in other $[SiP^{iPr}_3]RuX$ complexes, where X is a neutral or anionic ligand trans to the Si anchor in the $[SiP^{iPr}_3]$ scaffold (Table 2).[16] The elongation of the Ru−Si bond reflects an approach of the metal center toward a pseudotetrahedral geometry, with a corresponding weakening of the Ru−Si bond. This change in geometry has significant consequences toward its electronic structure (see Section 2.9). The Ru−N distance of

dx.doi.org/10.1021/ja211603f | J. Am. Chem. Soc. 2012, 134, 6695−6706

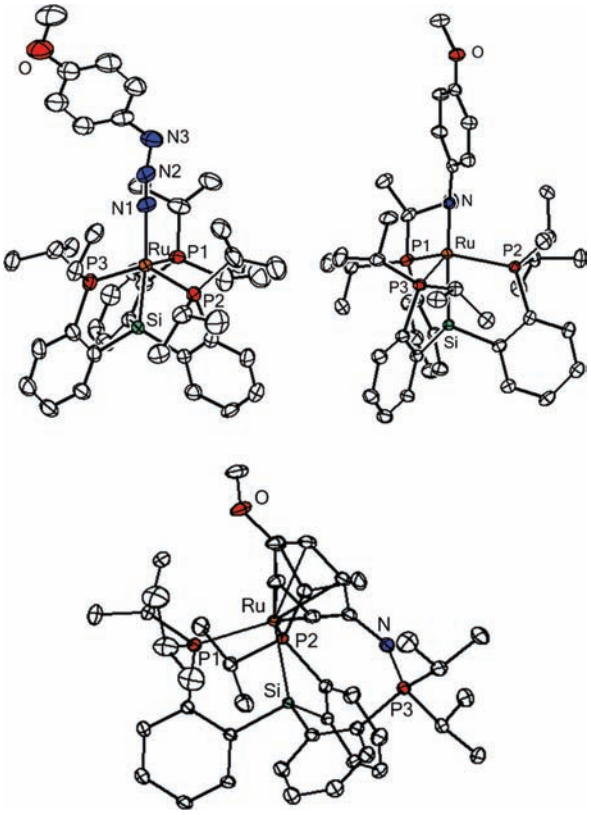

Figure 2. Solid-state structure of **8-OMe** (top, left), **7-OMe** (top, right), and **10** (bottom). Anions, hydrogen atoms, and solvent molecules are removed for clarity.

Table 2. Comparison of Ru−Si bond lengths (Å) and Sum of P−Ru−P Angles (°) for Representative 5-Coordinate Ru(I) and Ru(II) Complexes Relative to 7-OMe

	$[SiP^{iPr}_3]RuI$[a]	**4**[a]	**8-OMe**	**7-OMe**
Ru−Si (Å)	2.284(1)	2.319(1)	2.305(1)	**2.491(1)**
∑(P−Ru−P)	353.3(1)	352.7(1)	352.1(1)	**340.9(1)**

[a]From ref 16.

1.802(3) Å, while significantly shorter than in **5-CF$_3$**, is longer than the two other structurally characterized Ru(IV) imide complexes (1.716(3) and 1.785(6) Å).[18] The solid-state structure of **7-CF$_3$** is very similar to **7-OMe** (see SI).

Finally, the solid-state structure of **10** features a phosphinimide moiety resulting from NAr insertion of **7-OMe** into one of the M−P bonds. This complex is best described as a three-legged piano stool complex. Dechelation of one P atom results from its oxidation to a formally pentavalent phosphorus atom, and an η^6 interaction between the aryl ring and the metal center is observed with Ru−C distances ranging between 2.23 and 2.40 Å. These distances are within, if not slightly longer, than reported Ru−C(aryl) distances for ruthenium complexes with an η^6 coordinated anisole ligand.[22]

2.4. Synthesis of 5-OMe and Mechanistic Studies. The cyclic voltammetry of **7-OMe** is shown in Figure 3 and displays a reversible reduction event at −1.24 V and an irreversible reduction event at −2.17 V. The first wave is assigned to a formal Ru(IV) to Ru(III) reduction, as this wave is close to the formal Ru(IV)/Ru(III) couple of **7-CF$_3$**. The irreversible wave is assigned to a Ru(III)/Ru(II) redox event. The reversible nature of the first redox event indicates that the product

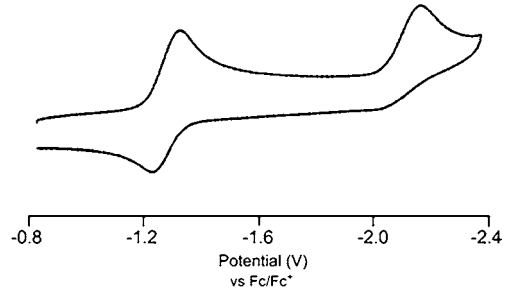

Figure 3. Cyclic voltammogram of **7-OMe**. Conducted in 0.3 M $TBAPF_6$ in THF.

resulting from one electron reduction of **7-OMe** is stable on the electrochemical time scale. Chemical reduction was accomplished by addition of 1 equiv of $CoCp_2$ to **7-OMe**, which caused a color change from green to red/brown. Removal of $[CoCp_2]PF_6$ and extraction into pentane led to the isolation of **5-OMe** in moderate yield. While its solid-state structure was not be obtained, the ^{1}H NMR of **5-OMe** is reminiscent of the spectrum of **5-CF$_3$**. The room temperature (RT) EPR spectrum (vide infra) of **5-OMe** is also similar to that of **5-CF$_3$**, corroborating its assignment. Interestingly, **5-OMe** is relatively stable at room temperature, showing signs of decomposition only after several hours in solution. Further, **5-OMe** does not produce azoanisole upon decay. These observations rule against a mechanism in common with the related Fe system, in which two imide species undergo N−N coupling (Scheme 6A).[10]

Scheme 6. Plausible Candidate Mechanisms for Liberation of Azoarenes Involving 5-OMe

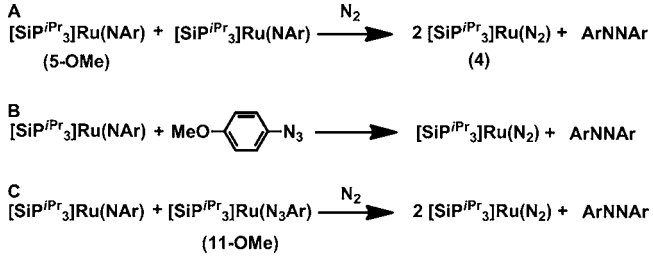

Other plausible mechanisms that involve **5-OMe** in the catalytic cycle are shown in Scheme 6B,C. In mechanism B, **5-OMe** reacts with free azide to yield azoanisole and **4**. This mechanism is related to one recently reported for a nickel system,[12b] in which azide addition to a nickel imide results in 1,3-dipolar addition to yield a tetrazene type intermediate/transition state that releases azoarene after N_2 extrusion. In mechanism C, **5-OMe** reacts with a transient Ru(I) azide adduct, $[SiP^{iPr}_3]Ru(N_3Ar)$ (**11-OMe**), to release azoanisole and regenerate **4**. To test the validity of mechanism B, *p*-$MeOC_6H_4N_3$ was added to **5-OMe**. Neither decay of **5-OMe** nor azoanisole formation was observed, ruling it out. To test mechanism C, a crossover experiment was designed with *p*-$EtOC_6H_4N_3$. First, a control experiment, in which a 1:1 mixture of *p*-$MeOC_6H_4N_3$ and *p*-$EtOC_6H_4N_3$ was added to **4**, was conducted. This reaction produced a statistical mixture of 1:2:1 ArNNAr/ArNNAr′/Ar′NNAr′ (Ar = *p*-$MeOC_6H_4$, Ar′ = *p*-$EtOC_6H_4$) (Scheme 7). Next, 1 equiv of *p*-$EtOC_6H_4N_3$ was added to 1 equiv each of **4** and **5-OMe**. If mechanism C was responsible for azoarene formation, the hetero azoarene,

dx.doi.org/10.1021/ja211603f | J. Am. Chem. Soc. 2012, 134, 6695−6706

Scheme 7. Reaction between 4 and a 1:1 Mixture of Two Similar Aryl Azides

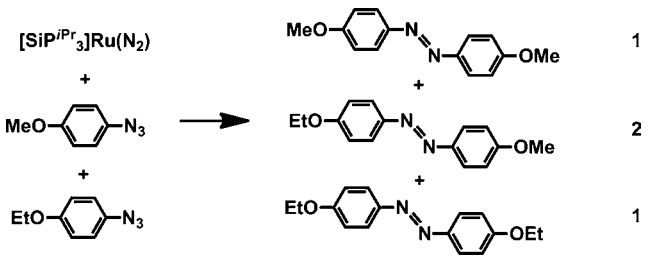

ArNNAr′, would be expected to form to some extent. In contrast, only the homocoupled azoarene, Ar′N═NAr′ (Ar′ = *p*-EtOC$_6$H$_4$) was observed (Scheme 8). This series of

Scheme 8. Crossover Experiment Discussed in the Text

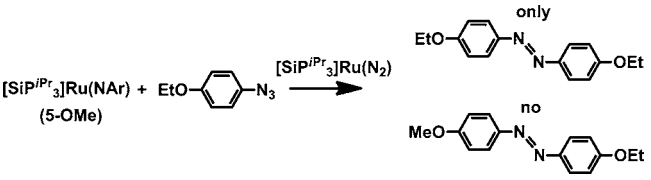

experiments rules out all three mechanisms that are shown in Scheme 6 and establish that the formally Ru(III) imide complex **5-OMe** is not involved in the catalytic cycle.

2.5. Considering the Release of Free Aryl Nitrene. An interesting alternative to the mechanistic scenarios shown in Scheme 6 is the release of aryl nitrene during the catalytic cycle from a ruthenium aryl azide precursor, **11-OMe**. It is well established that aryl nitrenes have triplet ground states[23] that react at near diffusion controlled rates with either themselves or with free aryl azide to produce azoarenes.[24] This reactivity is unique to the triplet state; singlet aryl nitrene is not known to form azoarene. In the present Ru system under consideration, because **4** and **11-OMe** both have doublet ground states (as shown by EPR spectroscopy, see Figure 5), both singlet and triplet nitrene could be released from **11-OMe** (Scheme 9). If

Scheme 9. Aryl Nitrene Release from 8-OMe

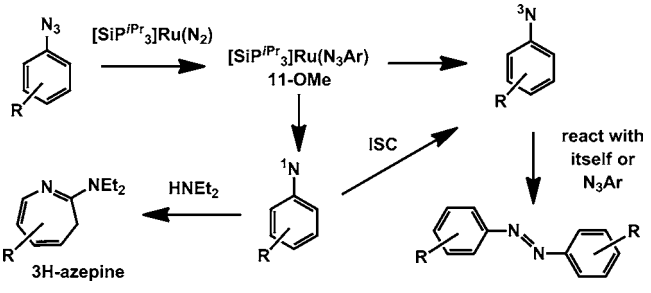

triplet nitrene is released, rapid recombination with itself or with free azide would yield azoanisole. If singlet nitrene is released, it could undergo intersystem crossing (ISC) to triplet nitrene to then produce azoanisole. This mechanism would be consistent with the absence of involvement of **5-OMe** and also with the results summarized in Scheme 7, where a statistical mixture of the three azoarenes is produced upon addition of a 1:1 mixture of two similar aryl azides to **4**.

Singlet aryl nitrenes have been trapped with nucleophiles such as diethyamine to yield azepine (Scheme 9).[25] Indeed, in our hands, generation of singlet nitrene by room temperature photolysis of tolylazide in neat diethylamine produced azepine as the major product as judged by GC−MS and ^{1}H NMR spectroscopy. A similar trapping experiment with *p*-MeOC$_6$H$_4$N$_3$ produced little, if any, azepine, possibly due to the >100-fold greater rate of ISC for this nitrene relative to singlet tolylnitrene.[23b] Thus, for the trapping experiment with **4**, tolyl azide was used instead of *p*-MeOC$_6$H$_4$N$_3$. Addition of tolyl azide to **4** in neat diethylamine, however, produced no azepine but only azotoluene. Thus, if singlet nitrene is released by **11-Me**, it must be undergoing ISC to the triplet state sooner than it is being trapped by diethylamine. In this case, ISC would have to be assumed to be accelerated by the influence of a nearby ruthenium center, since efficient trapping was established without the presence of ruthenium. Trapping of triplet nitrene is more difficult since most of the conventional triplet nitrene traps, such as nitrosobenzene,[26] would react with metalloradical **4**. Direct observation of triplet nitrene during the reaction by EPR spectroscopy was also considered. While photolysis of both tolylazide and *p*-MeOC$_6$H$_4$N$_3$ at 77 K in a frozen glass produced the EPR signal characteristic of triplet nitrene (Figure 4),[27] thawing at −78 °C resulted in rapid loss of

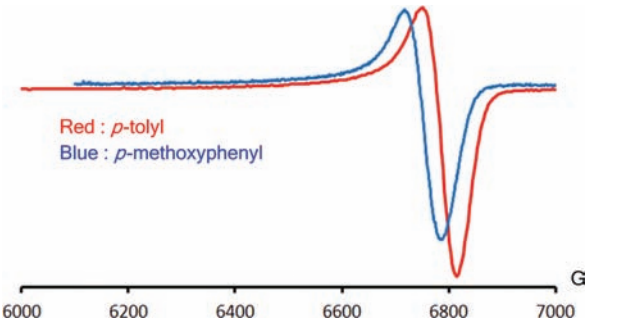

Figure 4. X-Band EPR spectra of triplet *p*-tolyl nitrene (red) and triplet *p*-methoxyphenyl nitrene (blue).

the signal within seconds. Thus, no buildup of triplent nitrene is expected, since the ruthenium catalyzed azoarene reaction is known only to take place at higher temperatures (vide supra).

2.6. EPR Spectroscopy on 5-R and 11-R. The room temperature and 77 K EPR spectra of **5-OMe** are shown in Figure 5. The room temperature spectrum depicts a three line pattern due to large coupling of 119 MHz to the nitrogen of the NAr moiety and smaller coupling of 48 MHz to one phosphorus atom. The N hyperfine coupling in **5-OMe** is larger relative to **5-CF$_3$** while the P coupling is smaller, which yields a combined effect of creating a three line pattern for **5-OMe** instead of a four line pattern as in **5-CF$_3$**.[16] Also worthy of note is the smaller Ru hyperfine coupling of 38 MHz, observed as satellites due to spin active isotopes of Ru (approximately 30%), in **5-OMe** relative to **5-CF$_3$** (48 MHz). Taken together, the hyperfine coupling to N and Ru indicate a greater spin density on the NAr moiety for **5-OMe** relative to **5-CF$_3$**. By analogy to the assignment of **5-CF$_3$** containing a NAr$^{\bullet-}$ radical moiety, we assign **5-OMe** as also possessing a NAr$^{\bullet-}$ radical.[4k,18b,28] The radical character on the NAr moiety is also supported from the isotropic *g*-value, g_{iso}, of 2.002, which shows little deviation from the value of the free electron, 2.0023. Further, the anisotropy in the *g*-values (Δg = 0.063) at 77 K is to be contrasted with the value for the Ru(I) metalloradical **4** (0.135) or the Ru(III) complex, {[SiP$^{iPr}_3$]-

dx.doi.org/10.1021/ja211603f | J. Am. Chem. Soc. 2012, 134, 6695−6706

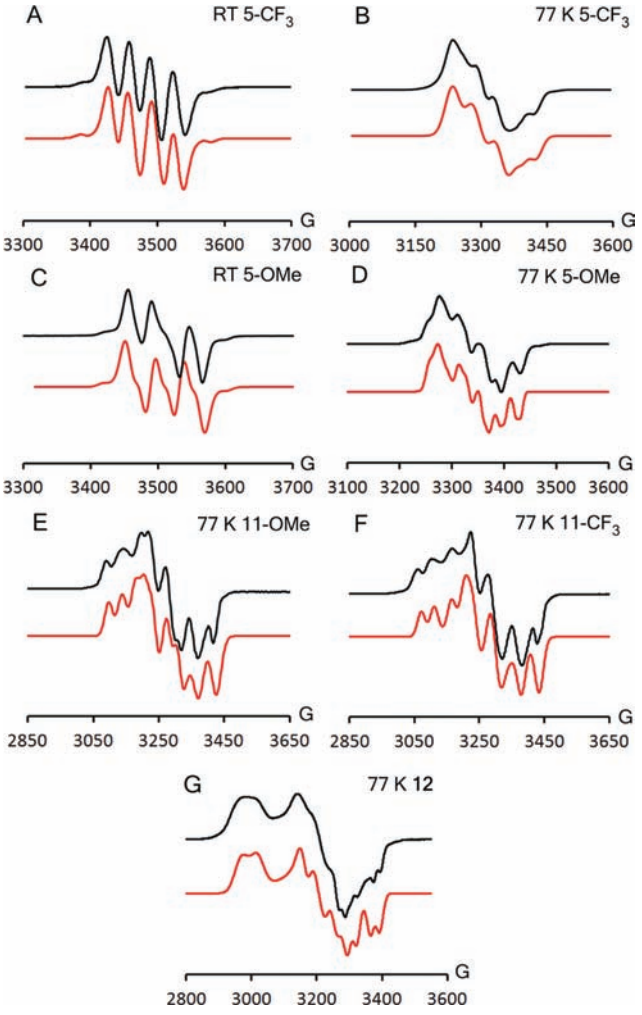

Figure 5. (A and B) EPR spectra of **5-CF$_3$** (A, RT; B, 77 K); (C and D) EPR spectra of **5-OMe** (C, RT; D, 77 K); (E) 77 K EPR spectrum of **11-OMe**; (F) 77 K EPR spectrum of **11-CF$_3$**; (G) 77 K EPR spectrum of **12**. For simulation parameters, see SI.

RuCl}PF_6 (**12**), which shows a Δg = 0.242. The latter complex was synthesized by oxidation of previously reported [SiP$^{iPr}_3$]-RuCl[16] with $AgPF_6$ and represents a formally Ru(III) metalloradical.

Measuring the RT EPR spectrum of the crude mixture from the stoichiometric reaction between **4** and *p*-$MeOC_6H_4N_3$ (Section 2.1) yielded a complicated spectrum. Deconvolution of the spectrum was performed by subtracting out the contribution from **4** and provided a spectrum of nearly pure **5-OMe**. This result suggests that, although **5-OMe** is not responsible for the catalysis of azoanisole formation, it is nevertheless formed under the reaction conditions. To probe whether complexes **5-R** (R = OEt, Me, Mes) were also formed during stoichiometric reactions, the RT EPR spectra of crude reaction mixtures were also measured (see Figure 6 for R = Me). Again, a complicated pattern was observed (Figure 6, SI), but similar deconvolution resulted in spectra similar to that of **5-OMe**. The results again point to distinct pathways that give rise to **5-R** and azoarene, in which the azoarene formation step is favored for more electron donating substituents.

As EPR proved to be a convenient tool in detecting minor amounts of paramagnetic products for this system, attempts were made to detect transient Ru(I) azide adducts, **11-R**, en

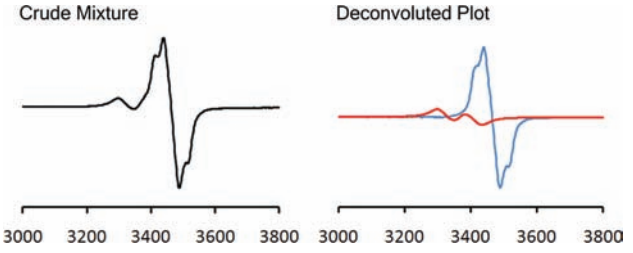

Figure 6. (Left) RT EPR spectrum of crude mixture from reaction between **4** and tolylazide. (Right) Contribution of **4** (red) and **5-Me** (blue) to crude spectrum. The blue line results from subtracting the contribution of the red line from the black experimental spectrum.

route to either **5-R** or azoarene at low temperature. To this end, a solution of 1 equiv of *p*-$CF_3C_6H_4N_3$ was layered over a frozen solution of **4**. The resulting layered frozen solution was rapidly thawed in a dry ice/isopropyl alcohol bath, quickly mixed, and frozen again for analysis by EPR spectroscopy. The EPR spectrum showed new signals that were distinct from **4**, but conversion was not complete. Addition of excess azide (>50 equiv) resulted in complete conversion to a new signal that was assigned as **11-CF$_3$** (Figure 5). Notably, the anisotropy in the *g*-values in this spectrum (Δg = 0.17) indicate significant metalloradical character (Figure 5). Similarly, addition of 1 equiv of tolylazide was enough to see new features attributable to **11-Me**, although excess was required for full conversion. In contrast, addition of 1 equiv of *p*-$MeOC_6H_4N_3$ led to unnoticeable changes in the EPR signatures of **4**, indicating the presence of an equilibrium between **4** and **11-OMe** that strongly favored **4**. Indeed, addition of over 50 equiv of *p*-$MeOC_6H_4N_3$ and evacuation of N_2 from the EPR tube was necessary for the signals of **11-OMe** to be observed. The direction of the equilibrium in this case appears to be dictated by the π-accepting properties of the aryl azide, since *p*-$MeOC_6H_4N_3$ is expected to be a better σ-donor than *p*-$CF_3C_6H_4N_3$.

Thawing a frozen solution of freshly prepared **11-CF$_3$** at −76 °C and recording the EPR spectrum as a function of time led to decay of **11-CF$_3$** to **5-CF$_3$** as shown in Figure 7. The decay followed first-order kinetics with a half-life of 23 min at −76 °C (Figure 8), and was independent of the concentration of *p*-$CF_3C_6H_4N_3$. The kinetics are consistent with N_2 extrusion from a transient Ru(I) azide adduct and corroborate the assignment

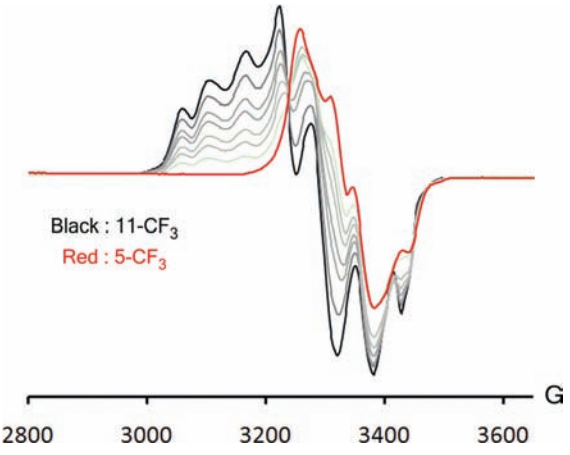

Figure 7. Decay of **11-CF$_3$** to **5-CF$_3$**. Black curve, **11-CF$_3$**; red curve, **5-CF$_3$**.

dx.doi.org/10.1021/ja211603f | J. Am. Chem. Soc. 2012, 134, 6695−6706

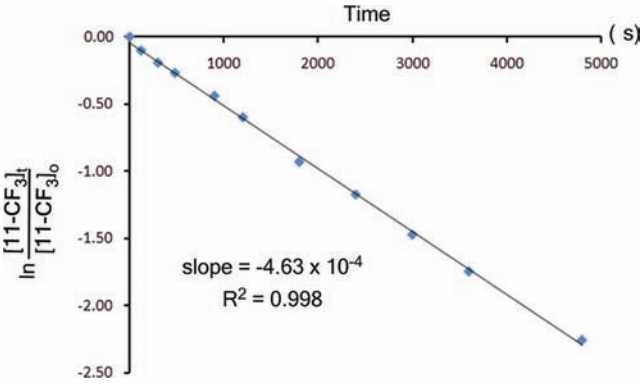

Figure 8. First-order decay plot of **11-CF$_3$** (3.4 mM) in 2-MeTHF at −76 °C. The value of $[\mathbf{11\text{-}CF_3}]_t/[\mathbf{11\text{-}CF_3}]_0$ was obtained by subtracting the contribution of **5-CF$_3$** from the experimental spectrum at each time and comparing the intensity of $[\mathbf{11\text{-}CF_3}]_t$ to $[\mathbf{11\text{-}CF_3}]_0$.

of **11-CF$_3$** as well as the assignment of **11-OMe**, which has similar EPR signatures.

2.7. DFT Calculations on 5-OMe and 11-OMe. DFT calculations on **5-OMe** and **11-OMe** were performed to further probe their electronic structures. The optimized structure of **5-OMe** is very similar to that of structurally characterized **5-CF$_3$**[16] and features a geometry that is between a TBP and SQP with τ = 0.44 (Figure 9). One of the P−Ru−P angles is considerably

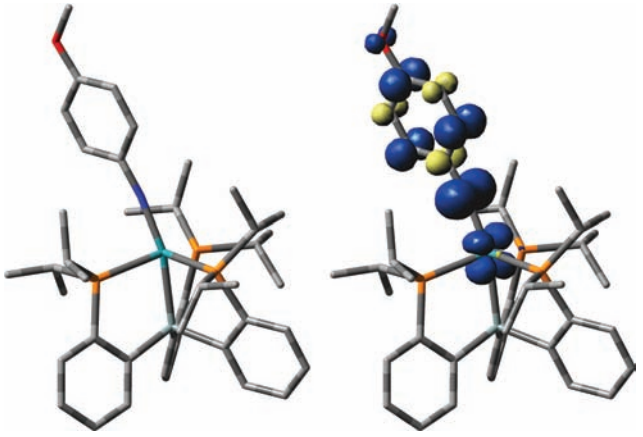

Figure 9. DFT optimized structure of **5-OMe** (left) and spin density plot (right).

larger (133.1°) than the other two and the NAr moiety is found to slightly slant into the pocket created by this large angle, giving rise to the observed distorted structure. The Ru−N distance is 1.887 Å, close to the optimized value for **5-CF$_3$** (1.872 Å). Previous DFT calculations on **5-CF$_3$** supported the EPR simulations that assigned a significant amount of spin density on the NAr moiety. The calculation on **5-OMe** also points to a similar conclusion. In fact, larger delocalization of spin density is seen on the NAr moiety (70%) for **5-OMe** relative to **5-CF$_3$** (54 %).[16] Conversely, the spin density on the metal center is lower (26% for **5-OMe** vs 40% for **5-CF$_3$**). These values are qualitatively consistent with the Ru and N hyperfine coupling constants found in the simulations of the RT EPR spectrum for **5-OMe** (Section 2.6).

The calculations on **11-OMe**, in contrast, support the EPR simulations that point to a metalloradical species. As the azide adduct may bind in several different modes, two η^1-bound structures (α and γ-bound) and two η^2-structures (α,β and β,γ-bound) were examined (Figure 10). Of these four isomers, the

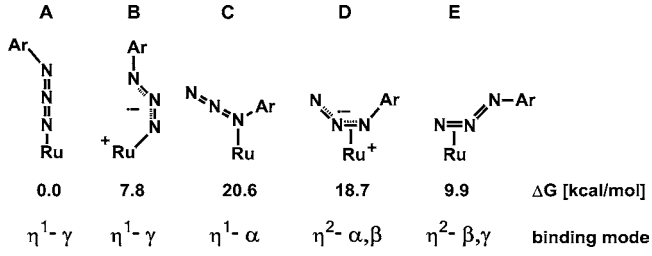

Figure 10. Energies of DFT optimized structures of **11-OMe**.

γ-bound azide adduct is found to be the most stable structure. Interestingly, two electronically distinct energy minima were found for the γ-bound structure. The lowest energy structure **A** shows localization of spin on the metal center, with little spread among the NAr moiety. In the optimized geometry, one P atom contains a much greater amount of spin density relative to the other two P atoms in the equatorial plane of the trigonal bipyramid; this trend is not noticeable for **5-OMe**, in which the radical is located in the NAr moiety and little spin density is distributed among the phosphines. This feature is consistent with the Ru(I) metalloradicals, **4** and $[\mathrm{SiP^{iPr}_3}]\mathrm{Ru(PMe_3)}$,[16] and the Group 9 metalloradicals, $\{[\mathrm{SiP^{iPr}_3}]\mathrm{M(PMe_3)}\}^+$ (M = Co, Rh, Ir).[29] The unequal spread in spin is reflected in the 77 K EPR spectrum, where only one P atom is found to be largely responsible for the fine features (Figure 5).

The second lowest energy structure (**B**) exhibits the same connectivity as **A** but differs by its electronic structure: 80% of its spin-density is located on the azide nitrogen atoms. The ligand radical character of **B** is inconsistent with the EPR spectrum, which exhibits large g-anisotropy suggestive of metalloradical character. However, the rather low energy difference (7.8 kcal/mol) indicates that such charge-transfer structures may be accessible and could in principle contribute to the observed reactivity. The α-bound azide adduct **C** was calculated less stable than the γ-bound adduct **A** by 20.6 kcal/mol (Figure 10), which must largely reflect the steric mismatch between the $[\mathrm{SiP^{iPr}_3}]$ scaffold and the aryl substituent; the unfavorable nature of the α-N binding mode is reflected in the long Ru−N distance of 2.568 Å. Of the two η^2-bound structures, the β,γ-structure **E** is more stable and only 9.9 kcal/mol above the energy of the γ-structure. This binding mode is rare but has precedent.[9] The geometry about the metal center is also rather close to that of the γ-structure, and the spin density distribution is found to be very similar. As a result, conclusive assignment of the ground state structure is difficult to make, and an equilibrium may even exist. The α,β-structure **D**, in turn, is 18.7 kcal/mol above the γ-structure, and exhibits large spin density (76%) on the unbound γ-N atom, while only 3% is found on the metal center. This electronic structure, similar to that of isomer **B**, is inconsistent with the EPR data. Overall, DFT calculations support the formulation of adducts **11** as terminally bound azide complexes of type **A** (Figure 10) with metalloradical character, in accord with the large g-anisotropy observed in the EPR spectrum.

2.8. Nitrene Release. Having established the η^1-γ-bound geometry **A** as the most likely ground state structure for azide adducts **11**, we located a transition state for the release of free triplet nitrene from the truncated model $[\mathrm{SiP^{Me}_3}]\mathrm{Ru(N_3Ph)}$ (Figure 11, see SI for details). An interesting feature of the

dx.doi.org/10.1021/ja211603f | J. Am. Chem. Soc. 2012, 134, 6695−6706

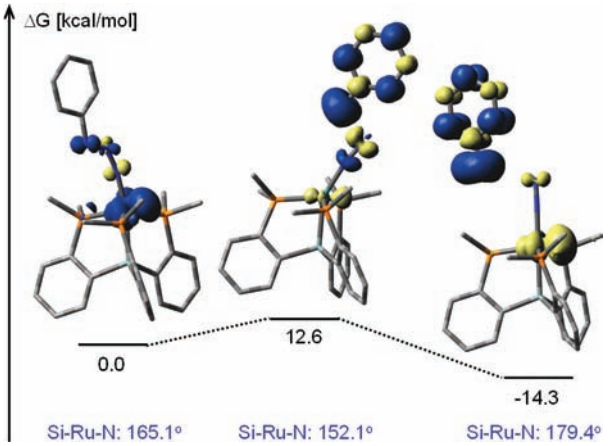

Figure 11. DFT-optimized transition state for the release of triplet phenylnitrene from $[SiP^{Me}_3]Ru(N_3Ar)$ and the corresponding spin densities.

calculated transition structure is the contraction of the Si−Ru−N angle to 152.1° versus 165.1° in the azide adduct and 179.4° in the final Ru−N_2 complex. This presumably increases the overlap between the Ru-centered SOMO and the π orbitals of the azide ligand, conferring some charge-transfer character to the transition state, as also suggested by inspection of the corresponding spin density (Figure 11). A quantitative interpretation of the free enthalpy of activation is difficult because of the limitations of single-determinantal DFT methods, but the calculated value of 12.6 kcal/mol is consistent with nitrene release from structure **A** being an accessible pathway. An alternative route involving the charge-transfer structure **B** as an intermediate cannot be ruled out, but overall the DFT study clearly substantiates the feasibility of ^{3}ArN release from Ru−N_3Ar adducts **11** to concomitantly liberate the Ru−N_2 complex **1**.

2.9. Electronic Structure of 7-OMe. Complex **7-OMe** is a trigonal bipyramidal, formally Ru(IV) complex with a d^4 electronic configuration. The thermal stability of this compound is striking given that a simplified molecular orbital diagram for a trigonal bipyramid (TBP) would place 4 electrons in π^* d_{xz} and d_{yz} orbitals, yielding a formal Ru−N bond order of 1. DFT calculations were thus performed to analyze the frontier orbitals of **7-OMe**. These calculations indicate that in contrast to a typical TBP MO diagram, the π^*orbitals, d_{xz} and d_{yz}, lie above the σ^* orbitals d_{xy} and $d_{x^2-y^2}$ (Figure 12). Accordingly, four electrons are placed in the $d_{xy}/d_{x^2-y^2}$ instead of the d_{xz}/d_{yz} orbitals, conserving a formal bond order of 3 for the Ru−N bond. The stability of **7-OMe** and the origin of the reversal of orbital ordering are likely due to the pyramidalization of the ruthenium center. The ruthenium is displaced out of the plane of the three phosphines, which leads to decreased P−Ru−P angles, an increased Ru−Si bond length (Table 2), and an approach of the complex toward a pseudotetrahedral geometry. The ample precedent for stabilization of multiply bonded metal complexes in late transition metals under pseudotetrahedral metal centers supports this argument.[30] Interestingly, the orbital located directly below the π^* orbitals possesses significant Si p_z and Ru d_{z^2} character. The overall MO diagram is very reminiscent of that of the recently reported [TPB]Fe(NAr) complex ([TPB] = (2-*i*Pr$_2$C$_6$H$_4$)$_3$B), Ar = *p*-C$_6$H$_4$OMe),[31] which features an iron center chelated by a tris(phosphino)borane ligand that is topologically related to the

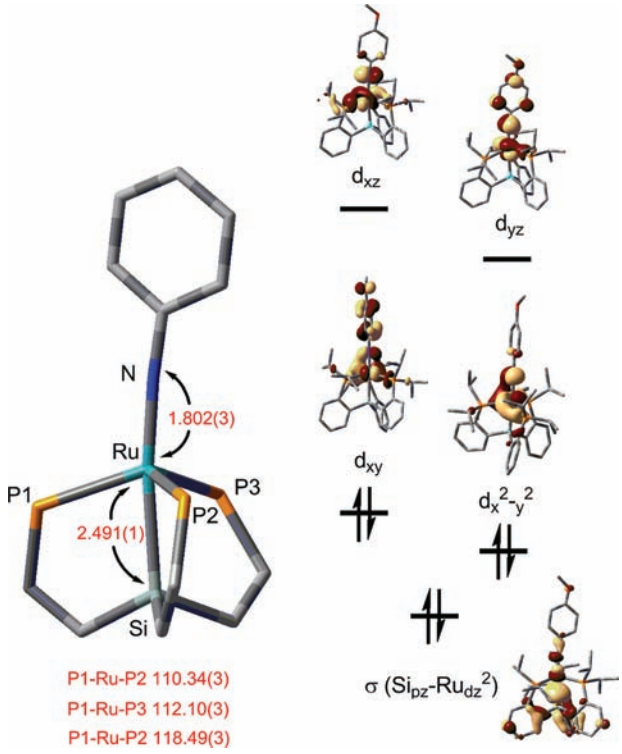

Figure 12. (Left) Core atoms of **7-OMe** with relevant bond lengths (Å) and angles (°). (Right) MO diagram of **7-OMe** obtained from a single point calculation on X-ray coordinates. The energy levels are drawn to scale. Calculated using the B3LYP functional with the LANL2TZ(f) for Ru and 6-311G** for all other atoms.

$[SiP^{iPr}_3]$ ligand. The metal center in this complex is more pyramidal than **7-OMe** (340.9°), with P−M−P angles summing to 330.0°. That the two complexes exhibit similar MO diagrams is perhaps expected as the [Fe−B] unit in [TPB]Fe(NAr) is valence isoelectronic to the $[Ru-Si]^+$ unit in **7-OMe** (Figure 13). One difference between these units is the

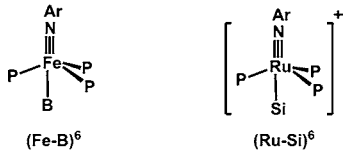

Figure 13. A comparison of [TPB]Fe(NAr) with **7-OMe**.

nature of the anchoring ligand; traditionally, silyl ligands are thought of as anionic electron donating ligands while boranes are considered neutral electron accepting ligands. While we continue to denote **7-OMe** as a formally Ru(IV) complex, the thought of the silicon atom acting as an electron acceptor (Si^+) in **7-OMe** is not unreasonable given the particularly low Ru(IV/III) redox potential of −1.24 V.

3. MECHANISTIC CONSIDERATIONS

Catalytic formation of azoarenes from aryl azides has little precedent. To our knowledge, the only example prior to our recent work on the $[SiP^{iPr}_3]$Fe system was reported by Cenini as a side reaction of catalytic C−H amination with Co porphyrins.[13] Recently, Heyduk[32] has reported a similar reaction. The work herein adds to the library of catalytic group transfer of two nitrene moieties to form azoarenes, and

dx.doi.org/10.1021/ja211603f | J. Am. Chem. Soc. 2012, 134, 6695−6706

showcases the first reaction chemistry mediated by the unusual Ru(I) oxidation state. Importantly, the mechanistic analysis in this work illustrates that the mechanism responsible for azoarene formation is distinct from the [SiP$^{iPr}_3$]Fe system. In Cenini's work, the azoarene is believed to form through the reaction between an imide complex of a cobalt porphyrin and a free organic azide (Scheme 10A). This mechanism is akin to

Scheme 10

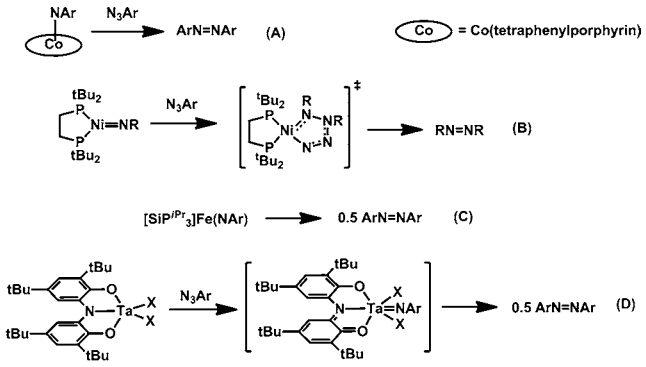

the reactivity observed in the stoichiometric azoarene formation mediated by a phosphine-supported Ni(II) center reported by Hillhouse (Scheme 10B).[12b] In contrast, the [SiP$^{iPr}_3$]Fe system invokes bimolecular coupling of two Fe(III) imide complexes; Heyduk's system also appears to operate through a related mechanism (Scheme 10C,D).[10,32] The experimental studies described in the present work rule out either of these mechanisms for the [SiP$^{iPr}_3$]Ru system. If a metal imide were involved, the catalytic cycle would involve a formal Ru(I)−N_2/Ru(III) NAr redox cycle, as in the [SiP$^{iPr}_3$]Fe system. This redox cycle is inconsistent with the mechanistic studies performed in this work, since **5-OMe** was detected in stoichiometric reactions and found to be stable over hours in solution while the catalytic azoarene formation in this system proceeds within seconds at room temperature. Moreover, independent synthesis of **5-OMe** as described above demonstrated that the decay product of **5-OMe** did not contain azoanisole. The Cenini type mechanism was also ruled out by observing that *p*-$MeOC_6H_4N_3$ does not yield any azoanisole on addition of **5-OMe**. Finally, crossover experiments described in Section 2.4 also ruled out a mechanism that involves a transient Ru(I) azide adduct, **11-OMe**, reacting with **5-OMe**. *Thus, 5-OMe does not appear to be responsible for azoarene formation at all.*

An alternative to consider is the release of free triplet nitrene from **11-OMe** (Scheme 11). After release of free triplet nitrene from **11-OMe**, it could react with itself or with free azide and yield azoanisole while regenerating **4** (Scheme 11). Such a mechanism would be consistent with the results in Scheme 7 and is additionally supported by the DFT optimization of a low-lying transition state for nitrene release (Figure 11) . The presence of **5-OMe** in the reaction mixture can be reconciled by the formation of a transient cage complex where the free nitrene is in the vicinity of the ruthenium. If the rate of nitrene capture by the metal fragment is rapid relative to nitrene escape from the cage, then the imide species, **5-R**, would be the major product. If cage escape is rapid, however, nitrene will escape and rapidly form azoarene. The different product distributions (**5-R** and azoarene) from altering the R group, from CF_3 to OMe, could be explained by the differing rates of nitrene

Scheme 11. Favored Mechanism for the Azoarene Catalytic Cycle

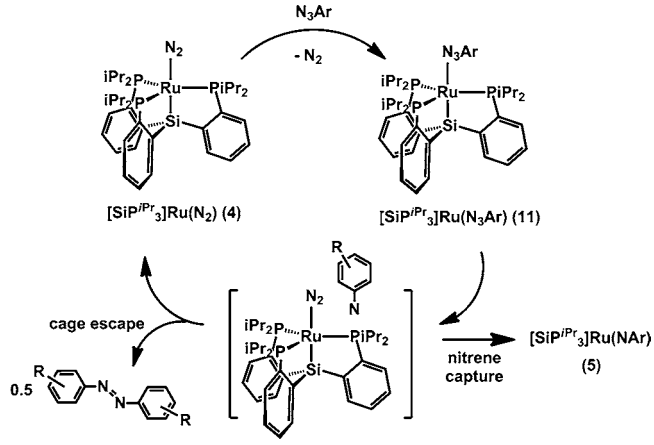

capture. The observation that **5-CF_3** is the sole product when *p*-$CF_3C_6H_4N_3$ is used is intuitively consistent with rapid nitrene capture, as nitrene capture formally involves a two electron oxidation of the metal center, which is expected to be facilitated by electron withdrawing groups on the aryl moiety.

One last mechanism to consider involves the reaction between **11-OMe** with itself or with free *p*-$MeOC_6H_4N_3$. This mechanism is conceptually related to the 'third oxidant' mechanism, as described by Goldberg in the oxygen atom transfer from iodosylarene to substrate by manganese corralazine complexes.[33] In this study, the often invoked Mn(V) oxo functionality was not found to be the source of the oxygen atom transferred to substrate; instead, the oxygen atom was transferred directly from a coordinated iodosylarene ligand. While we cannot rule this mechanism out, we disfavor it since the electronic polarization between the two reactants that exists in the Mn system does not exist in our system. Specifically, in the Mn corralazine study, the coordinated iodosylbenzene acts as the electrophile and substrate (olefin, sulfide) acts as the nucleophile, and thus, a distinct electronic polarization exists between the two. In our system, the transient Ru(I) azide adduct would need to act as both the nucleophile and electrophile, where such polarization is expected to be minimal. We thus favor the nitrene release mechanism.

4. CONCLUSIONS

In conclusion, we have demonstrated facile catalytic N−N coupling of aryl azides to yield azoarenes mediated by the Ru(I) metalloradical, [SiP$^{iPr}_3$]Ru(N_2) (**4**). Studies aimed at probing the viability of a bimolecular coupling mechanism of metal imide species as found in the related iron system have led to the isolation of several structurally unusual complexes, including the ruthenium imides, **5-OMe** and **7-OMe**, as well as the azide adduct **8-OMe**. Mechanistic studies showed that **5-OMe** is not involved in the catalytic cycle and demonstrates the influence of the metal center on the mechanism of reaction. Instead, we favor a mechanism in which free aryl nitrene is released during the catalytic cycle and combines with itself or with free aryl azide to yield the azoarene.

5. EXPERIMENTAL SECTION

5.1. General Considerations. All manipulations were carried out using standard Schlenk or glovebox techniques under an atmosphere of dinitrogen. Unless otherwise noted, solvents were degassed and

dx.doi.org/10.1021/ja211603f | J. Am. Chem. Soc. 2012, 134, 6695−6706

dried by thoroughly sparging with N_2 gas followed by passage through an activated alumina column. Hexamethyldisiloxane was dried over CaH_2 and distilled. Pentane, hexamethyldisiloxane, benzene, toluene, tetrahydrofuran, and diethylether were tested with a standard purple solution of sodium benzophenone ketyl in tetrahydrofuran. Unless noted otherwise, all reagents were purchased from commercial vendors and used without further purification. Celite (Celite 545) was dried at 150 °C overnight before use. Complexes **4**, **5-CF$_3$**, **9-BAr$^F_4$**, [SiP$^{iPr}_3$]RuCl were previously reported.[16] [$(C_6H_6)RuCl_2]_2$,[34] tris(2-(diisopropylphosphino)phenyl)silane ([SiP$^{iPr}_3$]H),[11] aryl azides,[35] and KC_8[36] were synthesized according to literature procedures. Triethylamine was dried over calcium hydride and distilled. Deuterated solvents were purchased from Cambridge Isotope Laboratories, Inc., degassed, and stored over 3-Å molecular sieves prior to use. Elemental analyses were performed by Midwest Microlabs. Varian Mercury-300 and Varian Inova-500 were used to collect ^{1}H, ^{13}C, ^{29}Si, and ^{31}P spectra at room temperature unless otherwise noted. ^{1}H and ^{13}C spectra were referenced to residual solvent resonances. ^{29}Si spectra were referenced to external tetramethylsilane (δ = 0 ppm), and ^{31}P spectra were referenced to external 85% phosphoric acid (δ = 0 ppm). IR measurements were obtained on samples prepared as KBr pellets using a Bio-Rad Excalibur FTS 3000 spectrometer. X-band EPR spectra were obtained on a Bruker EMX spectrometer. Spectra were simulated using Easyspin[37] program.

5.2. Crystallographic Details. X-ray diffraction studies were carried out at the Beckman Institute Crystallography Facility on a Brüker KAPPA APEX II diffractometer and at the MIT Department of Chemistry X-Ray Diffraction Facility on a Bruker three-circle Platform APEX II diffractometer solved using SHELX v. 6.14. The crystals were mounted on a glass fiber with Paratone-N oil. Data was collected at 100 K using Mo Kα (λ = 0.710 73 Å) radiation and solved using SHELXS[38] and refined against F^2 on all data by full-matrix least-squares with SHELXL. X-ray quality crystals were grown as described in the experimental procedures.

5.3. Electrochemical Details. Electrochemical measurements were carried out in a glovebox under a dinitrogen atmosphere in a one-compartment cell using a CH Instruments 600B electrochemical analyzer. A glassy carbon electrode was used as the working electrode and platinum wire was used as the auxiliary electrode. The reference electrode was Ag/$AgNO_3$ in THF. The ferrocene couple Fc+/Fc was used as an external reference. Solutions (THF) of electrolyte (0.3 M tetra-*n*-butylammonium hexafluorophosphate) and analyte were also prepared under an inert atmosphere.

5.4. Synthetic Details. *5.4.1. Synthesis of {[SiP$^{iPr}_3$]Ru(NAr)}OTf (Ar = p-C$_6$H$_4$CF$_3$) (7-CF$_3$).* [SiP$^{iPr}_3$]Ru(N_2) (100 mg, 0.14 mmol) was dissolved in 10 mL of Et_2O and cooled to −78 °C. *p*-$CF_3C_6H_4N_3$ (26 mg, 0.14 mmol) was diluted with 2 mL of Et_2O and also cooled to −78 °C. The azide solution was added dropwise to the solution of [SiP$^{iPr}_3$]Ru(N_2), resulting in an immediate color change from green to red/purple. The solution was stirred for 10 min at −78 °C and for 10 min at room temperature. The solution was cooled to −78 °C again, and AgOTf (36 mg, 0.14 mmol) was added in one portion. The solution gradually precipitated a green solid, along with black Ag metal. The mixture was filtered through Celite, and the green product was extracted into THF. The dark green solution was concentrated, and the product was recrystallized from layering pentane over a concentrated THF solution of green **7-CF$_3$** to yield crystals suitable for X-ray diffraction (82 mg, 59%). ^{1}H NMR (d_8-THF, δ): 8.31 (d, J = 8.0 Hz, 2H), 8.11 (d, J = 7.5 Hz, 3H), 7.77 (m, 3H), 7.59 (d, J = 8.5 Hz, 2H), 7.52 (t, J = 8.0 Hz, 3H), 7.41 (t, J = 7.5 Hz, 3H), 2.76 (br, 6H), 1.11 (dd, J = 14.5, 6.5 Hz, 18H), 0.52 (m, 18H). ^{13}C{^{1}H} NMR (d_8-THF, δ): 156.1, 141.2, 133.7, 132.0, 130.4, 129.2, 128.3, 120.8, 32.4, 19.5, 19.2. ^{19}F{^{1}H} NMR (d_8-THF, δ): −62.3, −77.3. ^{31}P{^{1}H} NMR (d_8-THF, δ): 109.8. Anal. Calcd for $C_{44}H_{58}NO_3F_6SiP_3SRu$: C, 51.96; H, 5.75; N. 1.38. Found: C, 51.59; H, 5.76; N, 1.25.

5.4.2. Synthesis of {[SiP$^{iPr}_3$]Ru(N$_3$Ar)}BAr$^F_4$ (8-OMe, Ar = C$_6$H$_4$OMe). {[SiP$^{iPr}_3$]Ru(N_2)}BAr$^F_4$ (46 mg, 0.029 mmol) was dissolved in 4 mL of Et_2O and cooled to −78 °C. *p*-$MeOC_6H_4N_3$ (4.4 mg, 0.029 mmol) was dissolved in 1 mL of Et_2O and also cooled to −78 °C. The azide solution was added dropwise to the {[SiP$^{iPr}_3$]Ru(N_2)}BAr$^F_4$ solution, which resulted in an immediate color change from orange to red. The solution was stirred at room temperature for 10 min and concentrated to yield red **8-OMe** (44 mg, 89%). Crystals suitable for X-ray diffraction were grown from layering pentane over a concentrated ether solution of **8-OMe** at −35 °C. ^{1}H NMR (d_8-THF, δ): 8.34 (d, J = 7.2 Hz, 3H), 7.79 (s, 8H), 7.64 (br, 3H), 7.57 (s, 4H), 7.47 (t, J = 7.2 Hz, 3H), 7.38 (t, J = 7.5 Hz, 3H), 7.16 (d, J = 9.0 Hz, 2H), 7.00 (d, J = 9.0 Hz, 2H), 3.78 (s, 3H), 2.10 (br, 6H), 1.17 (br, 18H), 0.83 (br, 18H). ^{13}C{^{1}H} NMR (d_8-THF, δ): 163.8 (m), 160.4, 154.4, 144.0, 136.5, 134.9, 131.6, 131.0, 130.8, 130.0, 129.6, 127.4, 123.1, 123.0, 119.1, 117.1, 67.2, 56.5, 20.8 (br), 16.5. ^{19}F{^{1}H} NMR (d_8-THF, δ): −61.2. ^{31}P{^{1}H} NMR (d_8-THF, δ): 72.9.

5.4.3. Synthesis of {[SiP$^{iPr}_3$]Ru(NAr)}BAr$^F_4$ (7-OMe). {[SiP$^{iPr}_3$]Ru(N_3Ar)}BAr$^F_4$ (**8-OMe**, Ar = C_6H_4OMe) (40 mg, 0.023 mmol) was dissolved in 2 mL of THF and charged in a 4 mL quartz cuvette. Excess *p*-$MeOC_6H_4N_3$ (4 mg, 0.027 mmol) was added to the cuvette and the red solution was photolyzed. The progress of the conversion was monitored by ^{31}P{^{1}H} NMR spectroscopy. After the conversion was complete (approximately 1 h), the green solution was concentrated, and the oily material was triturated with pentane (5 × 3 mL) to yield the green **7-OMe** (32 mg, 83%). Crystals suitable for X-ray diffraction were grown by layering pentane over a concentrated ether solution of **7-OMe** at −35 °C. ^{1}H NMR (d_8-THF, δ): 8.14 (d, J = 7.5 Hz, 3H), 7.78 (s, 8H), 7.77 (m, 3H), 7.57 (s, 4H), 7.44−6.85 (m, 10H), 3.83 (s, 3H), 2.74 (br, 6H), 1.12 (m, 18H), 0.55 (m, 18H). ^{13}C{^{1}H} NMR (d_8-THF, δ): 163.6 (m), 162.1, 157.2 (m), 142.6 (m), 136.5, 134.9, 133.0, 131.0, 130.8, 130.5, 130.2, 129.6, 127.5, 125.3, 125.2, 123.1, 119.1, 117.6, 57.1, 33.3, 20.5, 20.3.). ^{19}F{^{1}H} NMR (d_8-THF, δ): −61.4. ^{31}P{^{1}H} NMR (d_8-THF, δ): 106.4.

5.4.4. Synthesis of {[SiP$^{iPr}_3$]Ru(N_2)}PF$_6$ (9-PF$_6$), {[SiP$^{iPr}_3$]Ru(N$_3$Ar)}-PF$_6$ (8-OMe), and {[SiP$^{iPr}_3$]Ru(NAr)}PF$_6$ (Ar = C$_6$H$_4$OMe) (7-OMe). **9-PF$_6$**: [SiP$^{iPr}_3$]Ru(N_2) (35 mg, 0.048 mmol) was dissolved in 5 mL of THF. $AgPF_6$ (12 mg, 0.048 mmol) was dissolved in 1 mL of THF and both solution were cooled to −78 °C. The $AgPF_6$ solution was added dropwise to the solution of [SiP$^{iPr}_3$]Ru(N_2), causing an immediate darkening of the solution. The solution was stirred for 10 min, filtered through Celite, and concentrated. The solid was washed with Et_2O and dried to yield **9-PF$_6$** (31 mg, 74%). ^{1}H NMR (d_8-THF, δ): 8.25 (d, J = 6.9 Hz, 3H), 7.64 (d, J = 7.2 Hz, 3H), 7.42 (t, J = 6.9 Hz, 3H), 7.33 (t, J = 6.6 Hz, 3H), 2.44 (br, 6H), 1.22 (s, 18H), 0.86 (s, 18H). %). ^{13}C {1H} NMR (d_8-THF, δ): 155.2, 144.7, 134.2, 131.8, 131.0, 129.4, 29.3, 21.3, 20.5. ^{19}F{^{1}H} NMR (d_8-THF, δ): −72.9 (d, J = 715 Hz). ^{31}P{^{1}H} NMR (d_8-THF, δ): 67.5, −142.1 (sep, J = 715 Hz). **8-OMe, PF$_6^-$ anion**: {[SiP$^{iPr}_3$]Ru(N_2)}PF_6 (17 mg, 0.020 mmol) was dissolved in 6 mL of THF and cooled to −78 °C. *p*-$MeOC_6H_4N_3$ (2.9 mg, 0.020 mmol) was added to the solution in one portion, resulting in an immediate color change to red. The solution was stirred for 10 min, and concentrated to yield red **8-OMe** (18 mg, 94%). ^{1}H NMR (d_8-THF, δ): 8.26 (d, J = 7.0 Hz, 3H), 7.61 (br, 3H), 7.41 (t, J = 8.0 Hz, 3H), 7.32 (t, J = 8.0 Hz, 3H), 7.07 (d, J = 9.0 Hz, 2H), 6.97 (t, J = 9.0 Hz, 3H), 3.74 (s, 3H), 2.15 (br, 6H), 1.13 (s, 18H), 0.78 (s, 18H). ^{13}C{^{1}H} NMR (d_8-THF, δ): 159.8, 155.1, 144.5, 134.6, 132.8, 131.7, 131.3, 129.6, 122.6, 117.2, 56.6, 30.4, 21.2, 20.7. ^{19}F{^{1}H} NMR (d_8-THF, δ): −71.7 (d, J = 711 Hz). ^{31}P{^{1}H} NMR (d_8-THF, δ): 72.6, −142.9 (sep, J = 711 Hz). **7-OMe, PF$_6^-$ anion**: The synthesis of 7-OMe was performed in a three step sequence, without isolation of intermediate products, **9-PF$_6$** and **8-OMe**. [SiP$^{iPr}_3$]Ru(N_2) (50 mg, 0.068 mmol) was dissolved in 8 mL of THF. $AgPF_6$ (17 mg, 0.068 mmol) was dissolved in 2 mL of THF. Both were cooled to −78 °C and the $AgPF_6$ solution was added dropwise to the solution of [SiP$^{iPr}_3$]Ru(N_2), leading to an immediate color change from green to dark brown. The mixture was stirred at −78 °C for 5 min, and stirred at room temperature for 10 min. The mixture was filtered through Celite, and the filtrate was cooled to −78 °C. A THF solution of *p*-$MeOC_6H_4N_3$ (20 mg, 0.14 mmol) was added dropwise to the filtrate, resulting in a color change to red. The red solution of **8-OMe** was stirred for 10 min, and charged into a 100 mL quartz flask. The

dx.doi.org/10.1021/ja211603f | J. Am. Chem. Soc. 2012, 134, 6695−6706

solution was photolyzed and the progress of the reaction was monitored by $^{31}P\{^{1}H\}$ NMR spectroscopy. After the conversion was complete (approximately 1 h), the solution was concentrated, and the residues were washed with Et_2O to yield green **7-OMe** (57 mg, 86% overall). Recrystallization by layering pentane over a THF solution of **7-OMe** yielded crystals suitable for X-ray diffraction. ^{1}H NMR (d_8-THF, δ): 8.18 (d, J = 8.4 Hz, 2H), 8.12 (d, J = 7.2 Hz, 3H), 7.77 (m, 3H), 7.52 (t, J = 7.2 Hz, 3H), 7.41 (t, J = 6.9 Hz, 3H), 6.93 (d, J = 9.0 Hz, 2H), 3.85 (s, 3H), 2.76 (m, 6H), 1.11 (m, 18H), 0.55 (m, 18H). ^{13}C NMR (d^8-THF, δ): 162.3 (m), 157.3(m), 142.7 (m), 134.8 (m), 132.8, 131.2, 130.1, 125.5, 117.9, 57.3, 33.4 (m), 20.6, 20.3. ^{31}P NMR (d_8-THF, δ): 106.5, −143.6 (sep, J = 738 Hz). Anal. Calcd for $C_{43}H_{61}NOF_6SiP_4Ru$: C, 52.97; H, 6.31; N, 1.44. Found: C, 52.23; H, 6.18; N, 1.32.

*5.4.5. Synthesis of [SiP$^{iPr}_2$P(=NAr)Ru]PF$_6$ (**10**).* [SiP$^{iPr}_3$]Ru(N_2) (17 mg, 0.023 mmol) was dissolved in 5 mL of THF. $AgPF_6$ (5.8 mg, 0.023 mmol) was dissolved in 1 mL of THF. Both solutions were cooled to −78 °C and the $AgPF_6$ solution was added dropwise to the [SiP$^{iPr}_3$]Ru(N_2) solution, resulting in an immediate darkening of the solution. The mixture was stirred for 2 min at low temperature, and then stirred for 2 min at room temperature. The mixture was filtered through Celite, and the filtrate was cooled to −78 °C again. p-$MeOC_6H_4N_3$ (6.9 mg, 0.046 mmol) in 1 mL of THF was added to the solution dropwise, leading to a color change to red. The solution was stirred for 5 min, and charged into a 100 mL quartz flask. The solution was photolyzed for two days. The solution was concentrated, and washed with Et_2O to yield **10** (14 mg, 62%). Crystals suitable for X-ray diffraction were obtained by vapor diffusion of pentane into a concentrated solution of **10**. ^{1}H NMR (d_8-THF, δ): 7.92−7.83 (m, 2H), 7.66 (dd, J = 7.5, 4.2 Hz, 2H), 7.49 (d, J = 7.2 Hz, 2H), 7.43−7.23 (m, 6H), 6.66 (d, J = 6.0 Hz, 1H), 5.47 (d, J = 6.0 Hz, 1H), 5.31 (t, J = 6.9 Hz, 2H), 3.88 (s, 3H), 3.19 (sep, J = 6.6 Hz, 1H), 3.07 (sep, J = 5.7 Hz, 1H), 2.51−2.11 (m, 3H), 1.70−0.81 (m, 30H), 0.68 (dd, J = 14.7, 7.2 Hz, 3H), −0.33 (dd, J = 12.9, 7.8 Hz, 3H). $^{13}C\{^{1}H\}$ NMR (d_8-THF, δ): 155.2, 149.4 (d, J = 45.1 Hz), 148.1 (d, J = 15.7 Hz), 144.8 (d, J = 43.9 Hz), 142.4 (d, J = 13.2 Hz), 140.8, 137.3 (d, J = 17.3 Hz), 136.2 (d, J = 18.6 Hz), 134.2 (m), 132.7, 132.1 (d, J = 17.1 Hz), 131.1, 130.8, 130.3, 129.8, 129.1, 126.2, 116.0 (br), 90.9, 84.9, 81.8, 81.3, 81.2, 57.6, 56.6 (br), 35.9 (d, J = 29.2 Hz), 33.5 (d, J = 12.4 Hz), 32.3 (J = 18.9 Hz), 31.0, 30.4, 28.3, 27.9, 27.2, 24.4, 23.8, 23.4, 23.0, 21.4, 20.8, 20.0, 17.8, 17.7, 16.3, 2.2. $^{31}P\{^{1}H\}$ NMR (d_8-THF, δ): 85.4 (d, J = 28.3 Hz), 73.9 (d, J = 28.3 Hz), 32.4.

*5.4.6. Synthesis of [SiP$^{iPr}_3$]Ru(NAr) (Ar = C_6H_4OMe, **5-OMe**).* {[SiP$^{iPr}_3$]Ru(NAr)}PF_6 (Ar = C_6H_4OMe, **7-OMe**) (11 mg, 0.011 mmol) was dissolved in 4 mL of THF and cooled to −78 °C. $CoCp_2$ (2.0 mg, 0.011 mmol) was added in one portion and the resulting solution was stirred at −78 °C for 15 min. The solution was warmed to room temperature and stirred for an additional 15 min. The solution was concentrated, and the product was extracted into pentane. The pentane solution was filtered through Celite. The extraction process was repeated once more to yield red/brown **5-OMe** (4.6 mg, 52%). ^{1}H NMR (C_6D_6, δ): 9.0, 7.8, 6.8, 5.9, 4.0 (extending from 8 to 0 ppm). μ_{eff} (Evan's Method, C_6D_6/C_6H_6) = 1.5 μ_B. UV−vis (in THF): (nm, ε [mol^{-1} cm^{-1}]), 473 (4200), 737 (1700).

*5.4.7. Synthesis of {[SiP$^{iPr}_3$]RuCl}PF$_6$ (**12**).* [SiP$^{iPr}_3$]RuCl (30 mg, 0.040 mmol) was dissolved in 6 mL of THF. $AgPF_6$ (10 mg, 0.040 mmol) was dissolved in 1 mL of THF. Both were cooled to −78 °C and the $AgPF_6$ solution was added to the [SiP$^{iPr}_3$]RuCl solution. A gradual color change from red to brown took place. The solution was stirred at −78 °C for 15 min., and was subsequently stirred at room temperature for 30 min. The mixture was filtered through Celite, and the filtrate was concentrated. The residues were washed with ether and benzene, and the product was extracted into THF and filtered through Celite. Concentration of the purple filtrate yielded **12** (22 mg, 61%). ^{1}H NMR (CD_2Cl_2, δ): 12 (extending from 16 to 8 ppm), 9.7, 6.7, 6.4. μ_{eff} (Evan's Method, CD_2Cl_2) = 1.73 μ_B. UV−vis (in CH_2Cl_2): (nm, ε [mol^{-1} cm^{-1}]), 454 (290), 494 (1300). Anal. Calcd for $C_{36}H_{54}F_6SiP_4RuCl$: C, 48.62; H, 6.12; N, 0. Found: C, 47.95; H, 6.05; N, 0.00.

*5.4.8. Preparation of EPR Samples for Detecting Ru(I) Azide Adducts, **11-R**.* A solution of [SiP$^{iPr}_3$]Ru(N_2) (0.7 mg in 0.1 mL 2-MeTHF) was added to an EPR tube and the solution was frozen inside the glovebox using the glovebox cold well. A solution of azide (>30 equiv in 0.1 mL of 2-MeTHF) was layered above the frozen [SiP$^{iPr}_3$]Ru(N_2) solution and also frozen. The tube was quickly taken out of the glovebox and immersed in liquid nitrogen. The tube was immersed in a dry ice/isopropyl alcohol bath quickly to thaw the solution, and the tube was rapidly shaken to homogenize the solution. The tube was reimmersed in liquid nitrogen and frozen, and was placed inside the EPR cavity for measurement. For detecting **11-OMe**, several freeze−pump−thaw cycles were additionally applied to remove N_2 to favor formation of **11-OMe**.

■ ASSOCIATED CONTENT

Ⓢ Supporting Information

NMR spectra, EPR spectra with simulation parameters, DFT calculations, details of crystallographic data, and details of calculation methods and results. This material is available free of charge via the Internet at http://pubs.acs.org.

■ AUTHOR INFORMATION

Corresponding Author

jpeters@caltech.edu

Notes

The authors declare no competing financial interest.

■ ACKNOWLEDGMENTS

We acknowledge the generosity of NSF (Grant CHE-0750234) and the Gordon and Betty Moore Foundation for support of this work. M.-E.M. acknowledges a Fellowship for Advanced Researchers from the Swiss National Science Foundation. We also thank Dr. Hill Harman for insightful discussions. Dr. Peter Müller, Larry Henling, and Charlene Tsay provided crystallographic assistance.

■ REFERENCES

(1) Selected reviews: (a) Müller, P.; Fruit, C. *Chem. Rev.* **2003**, *103*, 2905. (b) Che, C.-M.; Lo, V. K.-Y.; Zhou, C.-Y.; Huang, J.-S. *Chem. Rev. Soc.* **2011**, *40*, 1950.

(2) Selected Examples: (a) Breslow, R.; Gellman, S. H. *J. Chem. Soc., Chem. Commun.* **1982**, 1400. (b) Breslow, R.; Gellman, S. H. *J. Am. Chem. Soc.* **1983**, *105*, 6728. (c) Mansuy, D.; Mahy, J. −P.; Dureault, A.; Bedi, G.; Battioni, P. *J. Chem. Soc., Chem. Commun.* **1984**, 1161. (d) Mahy, J. P.; Battioni, P.; Mansuy, D. *Tetrahedron Lett.* **1988**, *29*, 1927. (e) Evans, D. A.; Faul, M. M.; Bilodeau, M. T. *J. Org. Chem.* **1991**, *56*, 6744. (f) Müller, P.; Baud, C.; Jacquier, Y. *Tetrahedron* **1996**, *52*, 1543. (g) Albone, D. P.; Aujla, P. S.; Taylor, P. C.; Challenger, S.; Derrick, A. M. *J. Org. Chem.* **1998**, *63*, 9569. (h) Zhou, X.-G.; Yu, X.-Q.; Huang, J.-S.; Che, C.-M. *Chem. Commun.* **1999**, 2377. (i) Au, S.-M.; Huang, J.-S.; Yu, W.-Y.; Fung, W.-H.; Che, C.-M. *J. Am. Chem. Soc.* **1999**, *121*, 9120. (j) Kohmura, Y.; Katsuki, T. *Tetrahedron Lett.* **2001**, *42*, 3339. (k) Simkhovich, L.; Gross, Z. *Tetrahedron Lett.* **2001**, *42*, 8089. (l) Espino, C. G; Du Bois, J. *Angew. Chem., Int. Ed.* **2001**, *40*, 598. (m) Mar Díaz-Requejo, M.; Belderraín, T. R.; Carmen Nicasio, M.; Trofimenko, S.; Pérez, P. J. *J. Am. Chem. Soc.* **2003**, *125*, 12078. (n) Cui, Y.; He, C. *Angew. Chem., Int. Ed.* **2004**, *43*, 4210. (o) Zdilla, M. J.; Abu-Omar, M. M. *J. Am. Chem. Soc.* **2006**, *128*, 16971. (p) Milczek, E.; Boudet, N.; Blakey, S. *Angew. Chem., Int. Ed.* **2008**, *47*, 6825.

(3) A recent report describes the use of a hypervalent bromine reagent for the amination of unactivated C−H bonds. See; Ochiai, M.; Miyamoto, K.; Kaneaki, T.; Hayashi, S.; Nakanish, W. *Science* **2011**, *332*, 448.

(4) Selected examples: (a) Kwart, H.; Khan, A. A. *J. Am. Chem. Soc.* **1965**, *89*, 1951. (b) Cenini, S.; Tollari, S.; Penoni, A.; Cerada, C. *J.*

Mol. Catal. A: Chem. **1999**, *137*, 135. (c) Cenini, S.; Gallo, E.; Penoni, A.; Ragaini, F.; Tollari, S. *Chem. Commun.* **2000**, 2265. (d) Omura, K.; Murakami, M.; Uchida, T.; Irie, R.; Katsuki, T. *Chem. Lett.* **2003**, *32*, 354. (e) Omura, K.; Uchida, T.; Irie, R.; Katsuki, T. *Chem. Commun.* **2004**, 2060. (f) Li, Z.; Quan, R. W.; Jacobsen, E. N. *J. Am. Chem. Soc.* **1995**, *117*, 5889. (g) Liu, Y.; Che, C.-M. *Chem.—Eur. J.* **2010**, *16*, 10494. (h) Bach, T.; Körber, C. *Eur. J. Org. Chem.* **1999**, 1033. (i) Bach, T.; Körber, C. *Tetrahedron Lett.* **1998**, *39*, 5015. (j) Goa, G.-Y.; Jones, J. E.; Vyas, R.; Harden, J. D.; Zhang, X. P. *J. Org. Chem.* **2006**, *71*, 6655. (k) Badiei, Y. M.; Dinescu, A.; dai, X.; Palomino, R. M.; Heinemann, F. W.; Cundari, T. R.; Warren, T. H. *Angew. Chem., Int. Ed.* **2008**, *47*, 9961. (l) Stokes, B. J.; Dong, H.; Leslie, B. E.; Pumphrey, A. L.; Driver, T. G. *J. Am. Chem. Soc.* **2007**, *129*, 7500.

(5) (a) Proulx, G.; Bergman, R. G. *J. Am. Chem. Soc.* **1995**, *117*, 6382. (b) Proulx, G.; Bergman, R. G. *Organometallics* **1996**, *15*, 684.

(6) Gololobox, Y. G.; Zhmurova, I. N.; Kasukhin, L. F. *Tetrahedron* **1981**, *37*, 437.

(7) Fickes, M. G.; Davis, W. M.; Cummins, C. C. *J. Am. Chem. Soc.* **1995**, *117*, 6384.

(8) γ-N bound azide complexes: (a) Guillemot, G.; Solari, E.; Floriani, C. *Organometallics* **2001**, *20*, 607. (b) Evans, W. J.; Mueller, T. J.; Ziller, J. W. *J. Am. Chem. Soc.* **2009**, *131*, 2678. (c) Hanna, T. A.; Baranger, A. M.; Bergman, R. G. *Angew. Chem., Int. Ed. Engl.* **1996**, *35*, 653. α-N bound azide complex: (d) Barz, M.; Herdtweck, E.; Thiel, W. R. *Angew. Chem., Int. Ed. Engl.* **1998**, *37*, 2262. (e) Albertin, G.; Antonuitti, S.; Baldan, D.; Castro, J.; García-Fontán, S. *Inorg. Chem.* **2008**, *47*, 742. For a Cu complex that binds 1-adamantyl azide at the γ-N and a Ag complex that binds it at the α-N using the same ancillary ligand see, (f) Rasika Dias, H. V.; Polach, S. A.; Goh, S.-K.; Archibong, E. F.; Marynick, D. S. *Inorg. Chem.* **2000**, *39*, 3894.

(9) Waterman, R.; Hillhouse, G. L. *J. Am. Chem. Soc.* **2008**, *130*, 12628.

(10) Mankad, N. P.; Müller, P.; Peters, J. C. *J. Am. Chem. Soc.* **2010**, *132*, 4083.

(11) (a) Mankad, N. P.; Whited, M. T.; Peters, J. C. *Angew. Chem., Int. Ed.* **2007**, *46*, 5768. (b) Whited, M. T.; Mankad, N. P.; Lee, Y.; Oblad, P. F.; Peters, J. C. *Inorg. Chem.* **2009**, *48*, 2507. (c) Lee, Y.; Mankad, N. P.; Peters, J. C. *Nat. Chem.* **2010**, *2*, 558.

(12) (a) Hansert, B.; Vahrenkamp, H. *J. Organomet. Chem.* **1993**, *459*, 265. (b) Harrold, N. D.; Waterman, R.; Hillhouse, G. L.; Cundari, T. R. *J. Am. Chem. Soc.* **2009**, *131*, 12872.

(13) The only prior report was by Cenini, in which azoarene was a minor product of catalysis. See; Ragaini, F.; Penoni, A.; Gallo, E.; Tollari, S.; Gotti, C. L.; Lapadula, M.; Mangioni, E.; Cenini, S. *Chem.—Eur. J.* **2003**, *9*, 249.

(14) N—N coupling to yield azobenzenes from metal imide complexes: Zarkesh, R. A.; Ziller, J. W.; Heyduk, A. F. *Angew. Chem., Int. Ed.* **2008**, *47*, 4715.

(15) (a) Schröder, D.; Shaik, S.; Schwarz, H. *Acc. Chem. Res.* **2000**, *33*, 139. (b) Shaik, S.; Hirao, J.; Kumar, D. *Acc. Chem. Res.* **2007**, *40*, 532.

(16) Takaoka, A.; Gerber, L. C. H.; Peters, J. C. *Angew. Chem., Int. Ed.* **2010**, *49*, 4088.

(17) Dhuri, S. N.; Seo, M. S; Lee, Y.-M.; Hirao, H.; Wang, Y.; Nam, W.; Shaik, S. *Angew. Chem., Int. Ed.* **2008**, *47*, 3356.

(18) (a) Danopoulos, A. A.; Wilkinson, G.; Hussain-Bates, B.; Hursthouse, M. B. *Polyhedron* **1992**, *11*, 2961. (b) Walstron, A. N.; Fullmer, B. C.; Fan, H.; Pink, M.; Buschhorn, D. T.; Caulton, K. G. *Inorg. Chem.* **2008**, *47*, 9002.

(19) Takaoka, A.; Mendiratta, A.; Peters, J. C. *Organometallics* **2009**, *28*, 3744.

(20) Addison, A. W.; Rao, T. N.; Van Rijn, J. J.; Verschoor, G. C. *J. Chem. Soc., Dalton Trans.* **1984**, 1349.

(21) Select examples: (a) Klapötke, T. M.; Krumm, B.; Piotrowski, H.; Polborn, K.; Holl, G. *Chem.—Eur. J.* **2003**, *9*, 687. (b) Kawano, M.; Takayama, T.; Uekusa, H.; Ohashi, Y.; Ozawa, Y.; Matsubara, K.; Imabayashi, H.; Mitsumi, M.; Toriumi, K. *Chem. Lett.* **2003**, *32*, 922.

(22) Selected examples: (a) Hayashida, T.; Nagashima, H. *Organometallics* **2002**, *21*, 3884. (b) Kondo, T.; Tsunawaki, F.; Ura, Y.; Sadaoka, K.; Iwasa, T.; Wada, K.; Mitsudo, T. *Organometallics* **2005**, *24*, 905.

(23) (a) Schuster, G. B.; Platz, M. S. Photochemistry of Phenyl Azide. In *Advances in Photochemistry*; Volman, D., Hammond, G., Neckers, D., Eds.; John Wiley & Sons, Inc.; New York, 1992; Vol. *17*, p 69. (b) Platz, M. S. Nitrenes. In *Reaction Intermediate Chemistry*; Moss, R. A., Platz, M. S., Jones, M., Jr., Eds.; John Wiley & Sons, Inc.; New York, 2004; p 501.

(24) Reiser, A.; Willets, F. W.; Terry, G. C.; Williams, V.; Marley, R. *Trans. Faraday Soc.* **1968**, *64*, 3265.

(25) Borden, W. T.; Gritsan, N. P.; Hadad, C. M.; Karney, W. L.; Kemnitz, C. R.; Platz, M. S. *Acc. Chem. Res.* **2000**, *33*, 765.

(26) Liang, T.-Y.; Schuster, G. B. *J. Am. Chem. Soc.* **1987**, *109*, 7803.

(27) (a) Smolinsky, G.; Wasserman, E.; Yager, W. A. *J. Am. Chem. Soc.* **1962**, *84*, 3220. (b) Herbert Hall, J..; Fargher, J. A.; Gisler, M. R. *J. Am. Chem. Soc.* **1978**, *100*, 2029.

(28) Other complexes assigned as containing an radical on the NAr ligand: (a) Kogut, E.; Wiencko, H. L.; Zhang, L.; Cordeau, D. E.; Warren, T. H. *J. Am. Chem. Soc.* **2005**, *127*, 11248. (b) Lu, C. C.; George, S. D.; Weyhermüller, Bill, E.; Bothe, E.; Wieghardt, K. *Angew. Chem., Int. Ed.* **2008**, *47*, 6384. (c) King, E. R.; Hennessy, E. T.; Betley, T. A. *J. Am. Chem. Soc.* **2011**, *133*, 4917. (d) Lyaskovskyy, V.; Olivos Suarez, A. I. O.; Lu, H.; Jiang, H.; Zhang, X. P.; de Bruin, B. *J. Am. Chem. Soc.* **2011**, *133*, 12264.

(29) Takaoka, A.; Peters, J. C. *Inorg. Chem.* **2012**, *51*, 16.

(30) Sauouma, C.; Peters, J. C. *Coord. Chem. Rev.* **2011**, *255*, 920.

(31) Moret, M.-E.; Peters, J. C. *Angew. Chem., Int. Ed.* **2011**, *50*, 2063.

(32) Heyduk, A. F.; Zarkesh, R. A.; Nguyen, A. I. *Inorg. Chem.* **2011**, *50*, 9849.

(33) Wang, S. H.; Mandimutsira, B. D.; Todd, R.; Ramdhanie, B.; Fox, J. P.; Goldberg, D. P. *J. Am. Chem. Soc.* **2004**, *126*, 18.

(34) Palmer, M. J.; Kenny, J. A.; Walsgrove, T.; Kawamoto, A. M.; Wills, M. J. *J. Chem. Soc., Perkin Trans. 1* **2002**, 416.

(35) Hu, M.; Li, J.; Yao, S. Q. *Org. Lett.* **2008**, *10*, 5529.

(36) Weitz, I. S.; Rabinovitz, M. *J. Chem. Soc., Perkin Trans. 1* **1993**, 117.

(37) Stoll, S.; Schweiger, A. *J. Magn. Reson.* **2006**, *178*, 42.

(38) Sheldrick, G. M. *Acta Crystallogr.* **2008**, *A64*, 112.